Received: 24 July 2018 | Revised: 2 March 2019 | Accepted: 31 March 2019

DOI: 10.1111/apha.13278

REGULAR PAPER

ACTA PHYSIOLOGICA

miR-29c improves skeletal muscle mass and function throughout myocyte proliferation and differentiation and by repressing atrophy-related genes

William José Silva[1] | **Flavia Aparecida Graça**[1] | **André Cruz**[1] | **João Guilherme Silvestre**[1] | **Siegfried Labeit**[2] | **Elen Haruka Miyabara**[1] | **Chao Yun Irene Yan**[3] | **Da Zhi Wang**[4] | **Anselmo Sigari Moriscot**[1]

[1]Department of Anatomy, Institute of Biomedical Sciences, University of Sao Paulo, Sao Paulo, Brazil

[2]Faculty for Clinical Medicine Mannheim of the University of Heidelberg, Institute for Integrative Pathophysiology, Universitätsmedizin Mannheim, Mannheim, Germany

[3]Department of Cell Biology, Institute of biomedical Sciences, University of Sao Paulo, Sao Paulo, Brazil

[4]Department of Cardiology, Boston Children's Hospital, Harvard Medical School, Boston, Massachusetts

Correspondence
Anselmo Sigari Moriscot, Department of Anatomy, Institute of Biomedical Sciences, University of São Paulo, 2415, Av. Professor Lineu Prestes, Sao Paulo 05508-000, Brazil.
Email: moriscot@usp.br

Funding information
Leducq Foundation, Grant/Award Number: FLQ13CVD04; Sao Paulo Research Foundation (FAPESP), Grant/Award Number: 645648; National Institutes of Health, Grant/Award Number: HL085635 and HL116919; European Union for financial support (Horizon 2020 project Muscle Stress Relief network), Grant/Award Number: 645648; Conselho Nacional de Desenvolvimento Científico e Tecnológico

See Editorial Commentary: Falcone, G. 2019. A new role of miR-29c as a potent inducer of skeletal muscle hypertrophy. *Acta Physiol*. 226, e13320.

Abstract

Aim: To identify microRNAs (miRs) involved in the regulation of skeletal muscle mass. For that purpose, we have initially utilized an in silico analysis, resulting in the identification of miR-29c as a positive regulator of muscle mass.

Methods: miR-29c was electrotransferred to the tibialis anterior to address its morphometric and functional properties and to determine the level of satellite cell proliferation and differentiation. qPCR was used to investigate the effect of miR-29c overexpression on trophicity-related genes. C2C12 cells were used to determine the impact of miR-29c on myogenesis and a luciferase reporter assay was used to evaluate the ability of miR-29c to bind to the MuRF1 3′UTR.

Results: The overexpression of miR-29c in the tibialis anterior increased muscle mass by 40%, with a corresponding increase in fibre cross-sectional area and force and a 30% increase in length. In addition, satellite cell proliferation and differentiation were increased. In C2C12 cells, miR-29c oligonucleotides caused increased levels of differentiation, as evidenced by an increase in eMHC immunostaining and the myotube fusion index. Accordingly, the mRNA levels of myogenic markers were also increased. Mechanistically, the overexpression of miR-29c inhibited the expression of the muscle atrophic factors MuRF1, Atrogin-1 and HDAC4. For the key atrogene MuRF1, we found that miR-29c can bind to its 3′UTR to mediate repression.

Conclusions: The results herein suggest that miR-29c can improve skeletal muscle size and function by stimulating satellite cell proliferation and repressing atrophy-related genes. Taken together, our results indicate that miR-29c might be useful as a future therapeutic device in diseases involving decreased skeletal muscle mass.

KEYWORDS
atrophy, hypertrophy, miR-29c, myogenesis, skeletal muscle, trophicity

William José Silva and Flavia Aparecida Graça contributed equally to the work.

1 | INTRODUCTION

Approximately 40% of the total body mass is composed of skeletal muscles, which provide structural support and enable the body to maintain posture,[1] continuously ventilate the lungs via the intercostal and diaphragm muscles,[2] and finally allow the initiation of voluntary-directed movements of our bodies. The diverse types of skeletal muscles are endowed with a high plasticity, allowing them to adapt their size (through atrophy and hypertrophy) and function in response to various environmental stimuli.

Medically, it is of increasing importance that a chronic perturbation of the trophically supportive skeletal muscle signalling pathways through an inactive lifestyle, malnutrition, denervation and catabolism drive hormonal stimuli such as inflammatory cytokines and glucocorticoids and can lead to loss of muscle mass.[3] Accordingly, the mechanisms underlying this process include a shift towards proteolysis with activation of ubiquitin-mediated proteasomal (UPS) degradation, and of the autophagosome system.[4,5] Importantly, a plethora of atrophic signals induced by dexamethasone,[6] inflammatory cytokines[7] and denervation or cast immobilization,[8] all lead to transcriptional upregulation of the so-called atrogenes (in particular MuRF1 and MAFbx/Fbxo32, also called Atrogin-1). These atrogenes code for muscle catabolism by promoting E3 ubiquitin ligases.[9] Consistent with this model, null mice for either gene (MuRF1 or Atrogin-1) exhibit resistance to muscle mass loss under atrophic conditions.[8]

Skeletal muscle hypertrophy, in contrast to mass loss, is characterized by an increased size of pre-existing myofibres and elevated synthesis of de novo myofibrils. This is accomplished by a shift in balance towards muscle protein synthesis and away from protein degradation in adult mammals. Muscle hypertrophy-inducing anabolic signals include the IGF1/PI3K/Akt/mTOR pathway[10] and the myostatin-GDF11 signalling axis.[11,12]

In summary, a variety of genes responsible for muscle protein synthesis/degradation, myofibril assembly and also muscle metabolism become important when energy flows need to be fine-tuned in a coordinated fashion during hypertrophy-atrophy transitions. Here, microRNAs (miRs) are likely to play a key role in skeletal muscle adaptive responses[13,14] because miRs can signal to many genes in parallel. miRs are short (~22nt) non-coding RNA sequences that regulate gene expression by binding to the 3′ UTR (3′ untranslated region) of target mRNAs leading to their degradation or impaired translation. miRs are organized in families, normally associated with related structure and evolutionary origin, and their members can be identified by letters.[15]

A subset of these miRs, notably miR-1, miR-133a/b, miR-206, miR-208b and miR-499, are enriched in striated muscle, are key players in skeletal muscle plasticity and have an important role in the myoblasts differentiation process, muscle regeneration and muscle fibre identity.[16] Therefore, they have been defined as myomiRs.[17,18] Nonetheless, it is expected that these myomiRs are not the only players involved in the regulation of skeletal muscle function. Indeed, it has been shown that other miRs, such as miR-23a, can regulate muscle biology by reducing MuRF1 and MuRF2 mRNA levels and are sufficient to mitigate muscles from atrophy.[19] Other authors have shown that miR-27a inhibits myostatin mRNA, leading to skeletal muscle hypertrophy and satellite cell activation.[20] Taken together, these data highlight that miRs play a key role in skeletal muscle plasticity and that the identification and characterization of additional miRs will contribute towards to our knowledge of this complex biological process.

In the present study, we searched for novel skeletal muscle regulatory miRs by in silico analysis and functional validation. Our initial strategy focused on searching for miR families that have a high incidence of predicted targets in mRNAs involved in skeletal muscle mass control. Of the 26 miR families identified, we concentrated our efforts on characterizing miR-29c, because the miR-29 family was one of the top-rated miR families in our in silico analysis, and particularly miR-29c has been reported to play a role in myogenesis.[21] Importantly, mature miR-29s share identical seed regions, whereas different flanking regions confer miR-29 specificity. Finally, miR-29b has recently been implicated in driving atrophy by increasing the expression of MuRF1 in several types of muscle atrophy in vitro and in vivo.[22] The miR-29 family comprises miR-29a and miR-29b-1, which are clustered on chromosome 4, and miR29b-2 and miR29c, which are clustered on chromosome 13.[23] The miR29b-1 sequence is identical to that of miR29b-2. In the context of myogenesis, the miR-29 family has been shown to participate in a negative feedback loop involving components of the PcG (Polycomb Group), which drives epigenetic inhibition of MyoD and Myogenin during myogenesis.[24] Furthermore, the miR-29 family can also promote differentiation by repressing AKT3 in myocytes.[25]

Here, we show that the overexpression of miR-29c in the mouse tibialis anterior triggers an approximately 40% increase in mass gain, with an equivalent increase in maximal tetanic force. In addition, miR-29c overexpression decreases the mRNA levels of Atrogin-1, MuRF1 and HDAC4. Overall, the results suggest that miR-29c plays an important role in skeletal muscle hypertrophy and might be useful as a therapeutic device in the future to address conditions with altered muscle trophicity.

2 | RESULTS

2.1 | Identification of the miR-29 family as regulators of skeletal muscle hypertrophy and atrophy

Our first goal was to identify miR families that have the potential to modulate muscle trophicity in a pleiotropic fashion

by targeting multiple muscle mRNAs. To accomplish this, we first generated a list of mRNAs notoriously involved with multiple pathways as baits, including IGF1, IRS1, PI3K, AKT, mTOR, NFATC, HDCA4, JNK1, FOXO3, Atrogin-1, MuRF-1, myostatin, GSK3, LATS1 and SGK1 (for a full list of genes, see Table S1). For these genes, TargetScan identified putative regulatory miR families that were rated based on the number of mRNA hits obtained (a minimum of six hits was considered for rating, Table 1). Notably, we have considered only miR families conserved in mammals. Subsequently, we decided to address the miR-29 family, the second top-rated miR family previously described as being involved in skeletal muscle differentiation.[24,26,27] The miR-340 family was rated in the first position (Table 1), and we are currently addressing this miR in a separate study. Regarding the miR-29 family, recently one of its members, miR-29b, has already been implicated in the control of skeletal muscle mass.[22] The miR-29b coding sequence is located in a cluster on chromosome 13 along with miR-29c, leading us to start the investigation with miR-29c.

2.2 | Overexpression of miR-29c results in skeletal muscle structural alterations

Next, we electrotransferred a pMIR29c expression vector into the tibialis anterior to evaluate the impact of miR-29c increased levels of skeletal muscle in vivo. The efficiency of transgene expression was determined by GFP immunodetection and miR-29c qPCR analysis. GFP staining was detected at 4 and 7 days after electrotransfer in the empty vector (EV) and pMIR29c groups (Figure 1A). Our results show that approximately 30% and 75% of the fibres were GFP-positive 4 and 7 days after electrotransfer, respectively (Figure 1B,C). In contrast, no GFP-positive signal was detected in naive controls or negative controls (Figure 1A). miR-29c expression was elevated approximately 1.65-fold 7 days and 1.75-fold 30 days after electrotransfer, when compared to that in the EV group (Figure 1D).

TABLE 1 microRNAs predicted to influence skeletal muscle mass

microRNA Families	Hits
340	18
29	16
182	14
124/128/144/181/23/27/9	11
135/140/186/30/374	10
153/495	9
137/203/320/330	8
19/223/377/448/506	7

While electrotransfer of EV did not cause significant alterations in skeletal muscle mass when compared to the naive control group, the overexpression of miR-29c (30 days after electrotransfer) substantially increased the mass of the tibialis anterior by 40% when compared to the EV group (Figure 2A and Table S2). This result was paralleled by increased fibre cross-sectional area (CSA) (Figure 2B,C). In addition, the overexpression of miR-29c increased the median value of CSA distribution and augmented the maximum CSA value, generating fibres as large as 8050 μm^2 compared to the EV group (Figure 2C). In contrast, the EV group predominantly exhibited fibres with smaller diameters, ranging from 1050 to 3050 μm^2 (Figure 2C). Histological analysis of HE-stained sections showed many centralized nuclei and a higher incidence of split fibres in miR-29c-electrotransferred fibres (Figure 2B). Quantification of these features showed a substantial increase (3.3-fold) in the incidences of centralized nuclei (Figure 2D) and split fibres in the miR-29c-overexpressing group (approximately threefold, see Figure 2E) compared with those in the EV group. In the miR-29c-overexpressing group, there was a positive correlation between fibre area and the number of split fibres (Figure 2F). Taken together, these characteristics indicate that miR-29c overexpression (30 days after electrotransfer) caused intense tissue remodelling in skeletal muscle. We also measured the number of serial sarcomeres and noted that miR-29c-overexpressing muscles had an ~30% increase in this parameter as compared to that in the EV group. Accordingly, we detected a decrease in sarcomere length with similar intensity (~20%) in the miR-29c-overexpressing group when compared to that in the EV group (Figure 2G,H).

To unravel the cellular mechanisms underlying miR29c-driven hypertrophy, we first investigated cell proliferation through the quantification of Ki-67-positive nuclei. Ki67 is highly expressed in all cells engaged in the cell cycle and is therefore an excellent marker of the overall proliferation levels.[28] We detected extremely high levels of Ki-67-positive cells 4 days after miR-29c electrotransfer, (~4.5-fold higher than those in the EV group). The number of Ki-67-positive cells increased ~twofold 7 days after electrotransfer (Figure 3A,B) and returned to EV group levels 30 days after miR-29c electrotransfer (Figure 3A,B). We also investigated whether miR-29c-induced hypertrophy was specifically related to satellite cell proliferation and differentiation. To accomplish this, we performed an immunolabelling for Pax7 and MyoD, two factors strictly found in muscle satellite cells during activation/proliferation and compromised with the myogenic programme.[29] Indeed, miR-29c overexpression significantly increased the number of Pax7-positive nuclei, which peaked as early as 4 days after electrotransfer (~2.5-fold, Figure 4A,B). miR-29c overexpression also caused an increase in the number of MyoD-positive nuclei, which did not peak until 7 days after electrotransfer (~threefold, Figure 4C,D).

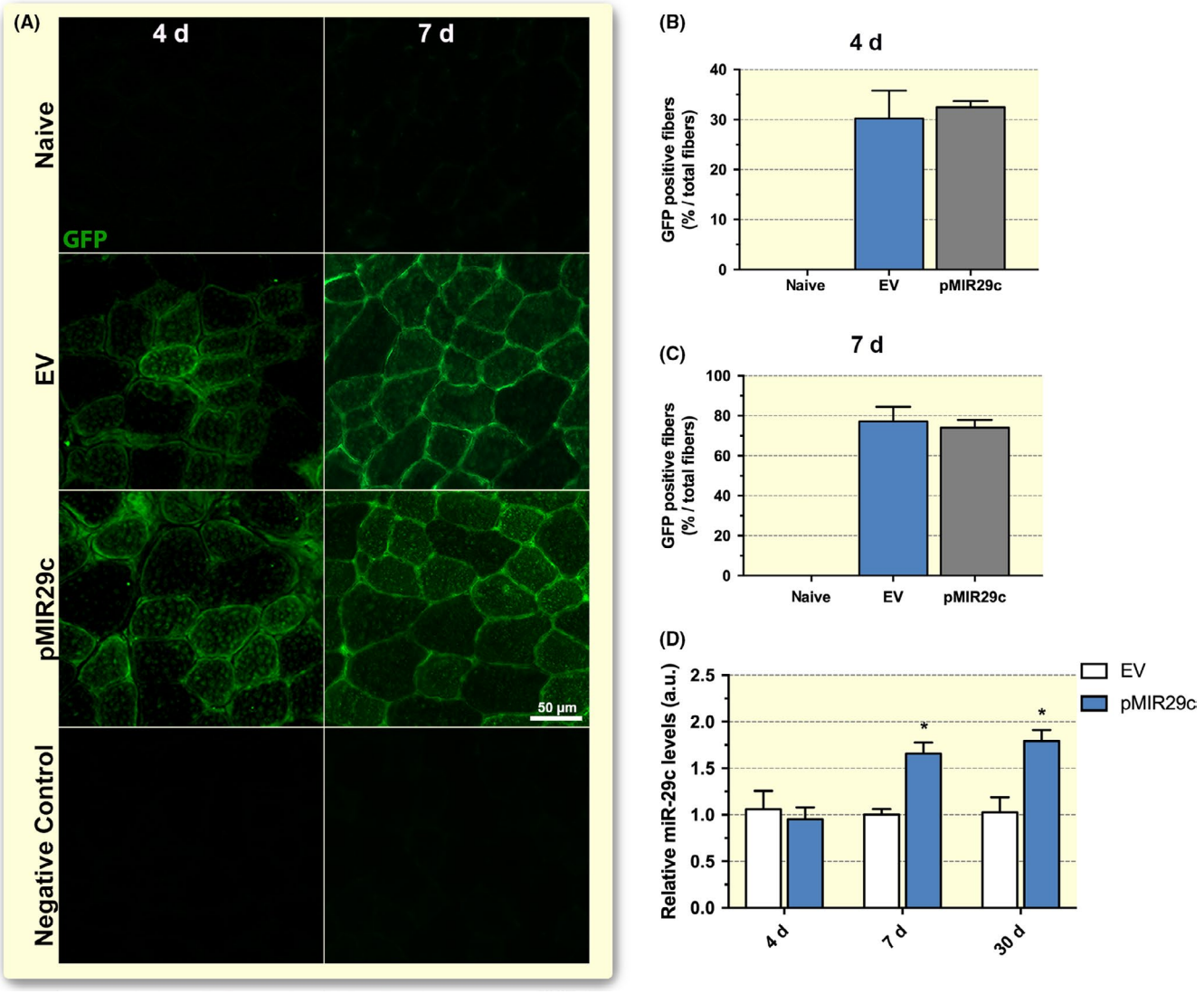

FIGURE 1 Overexpression of miR-29c by electrotransfer. Adult TA muscles from mice were injected with either empty vector (EV) or pMIR29c plasmids (GFP reporter co-expression) and gene delivery was induced by electrotransfer. (A) Representative immunofluorescence images of GFP in EV, pMIR29c and a naive group, in TA sections 4 or 7 days after electrotransfer. GFP-positive fibres (green) and DAPI for nuclei identification (blue). A control without primary antibody is also shown (Negative control). (B and C) Relative number of GFP-positive fibres/total fibres in naive, EV and pMIR29c 4 days (B) and 7 days (C) after electrotransfer (n = 4 per group). (D) RNA levels of miR-29c were determined by qPCR in the muscles 4, 7 or 30 days after electrotransfer. Data were expressed in percentage of total fibers and arbitrary units (au) as mean and SEM (n = 4 per group) and were corrected by the endogenous snoRNA234 RNA. Statistical analysis included one-way ANOVA followed by a Tukey's posttest. *$P \leq 0.05$ vs the respective EV group

In summary, our studies indicate that the overexpression of miR-29c promoted increased skeletal muscle mass, CSA and stimulated cell proliferation through the activation of satellite cells. We next investigated whether these alterations have a functional relevance.

2.3 | Overexpression of miR-29c enhances skeletal muscle contractile force

Next, we tested whether miR-29c electrotransfer could alter skeletal muscle function by evaluating transfected muscles 30 days after electrotransfer (Figure 5). Consistent with the positive impact of miR-29c overexpression on muscle mass, we observed an increase in the maximum tetanic force (~40%) as compared to that in the EV group (Figure 5A), whereas during a fatigue-simulating protocol, the maximum tetanic force decreased similarly in themiR-29c-overexpressing muscles and in the EV muscles (Figure 5B). Thus, although the maximum tetanic force in the miR-29c-overexpressing group was elevated as compared to that in the EV group, the specific forces were similar in both groups (Figure 5C,D). miR-29c-overexpressing muscles also developed increased

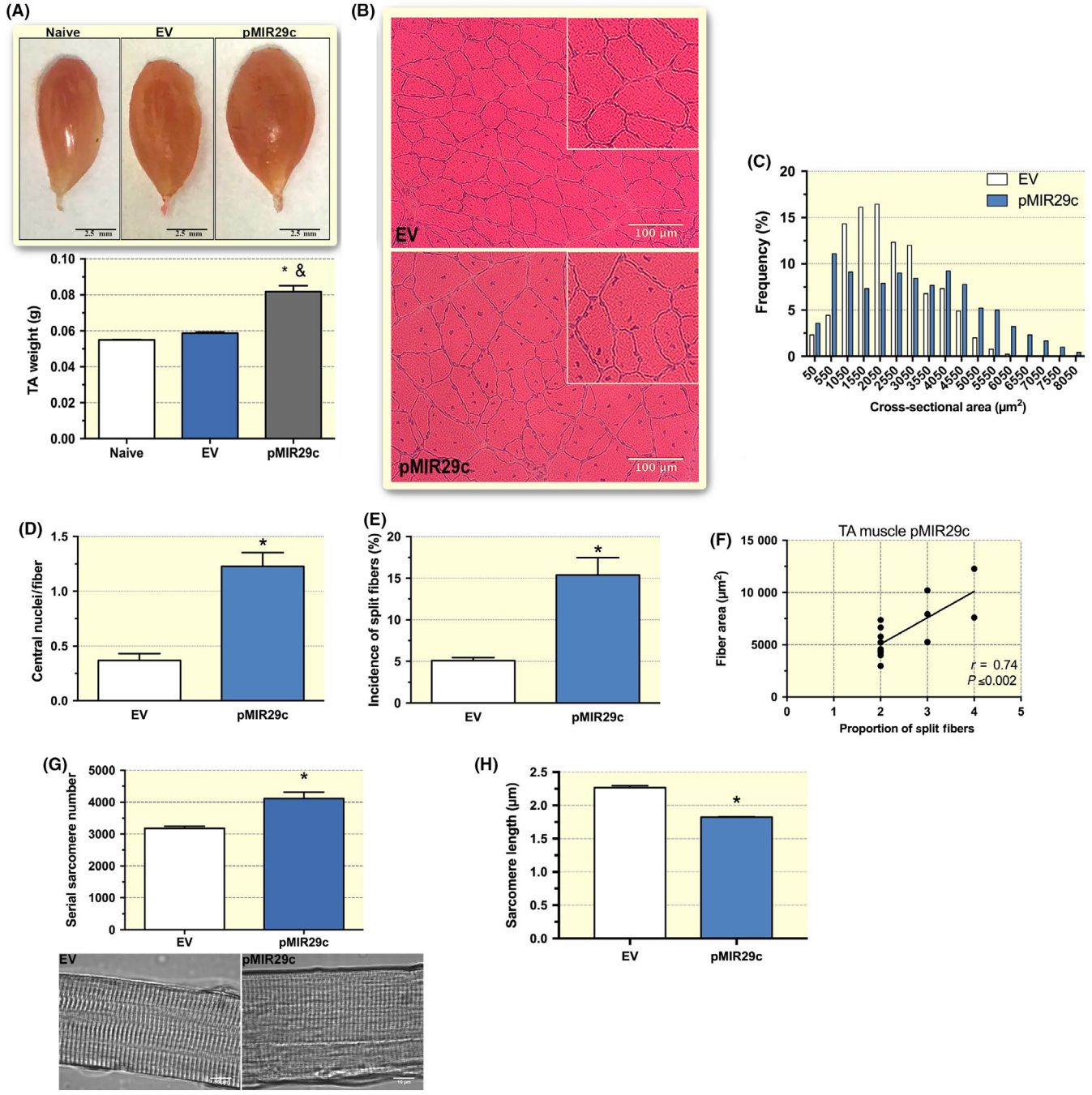

FIGURE 2 miR-29c induces muscle hypertrophy in vivo 30 days after electrotransfer. (A) Representative photographs and measurements of tibialis anterior (TA) mass from naive, empty vector (EV) and pMIR29c overexpression vector groups (n = 6 per group). (B) Representative hematoxylin-eosin (HE) staining from EV and pMIR29c overexpression vector groups. Inserts on the upper right of the micrographs highlight the tissue architecture of each group (n = 4 per group, scale bar 100 µm). (C) Quantification of muscle fibre cross-sectional area (CSA) distribution from EV and pMIR29c overexpression vector groups (n = 6 per group). TA was evaluated after the assessment of 900 fibres per animal and the Kolmogorov-Smirnov test was used, and significant difference ($P < 0.05$) was found between the miR-29c and EV groups. (D) Quantification of centralized nuclei per fibre in EV and pMIR29c groups. The number of total central nuclei evaluated in 300 fibres per animal was counted; n = 4 (E) Determination of the percentage of split fibres in EV and pMIR29c-overexpression vector groups; n = 4 and (F) also correlation between split fibre proportion and fibre CSA was determined. The proportion of split fibres in 300 fibres per animal was evaluated (Pearson correlation coefficient r = 0.74, $P \leq 0.002$); n = 4. (G) Measurements of serial sarcomere number of EV and pMIR29c overexpression vector groups and representative contrast phase photomicrographs are shown below (number of sarcomeres in series was measured within 300µm per fibre, n = 4, 6 fibres per animal). (H) Measurements of sarcomere length of EV and pMIR29c overexpression vector groups. Data are expressed as mean ± SEM. With the exception of C and F, an unpaired, two-tailed Student's *t* test was used for comparisons between two groups. $^{\&}P < 0.05$ vs naive. $^{*}P < 0.05$ vs EV

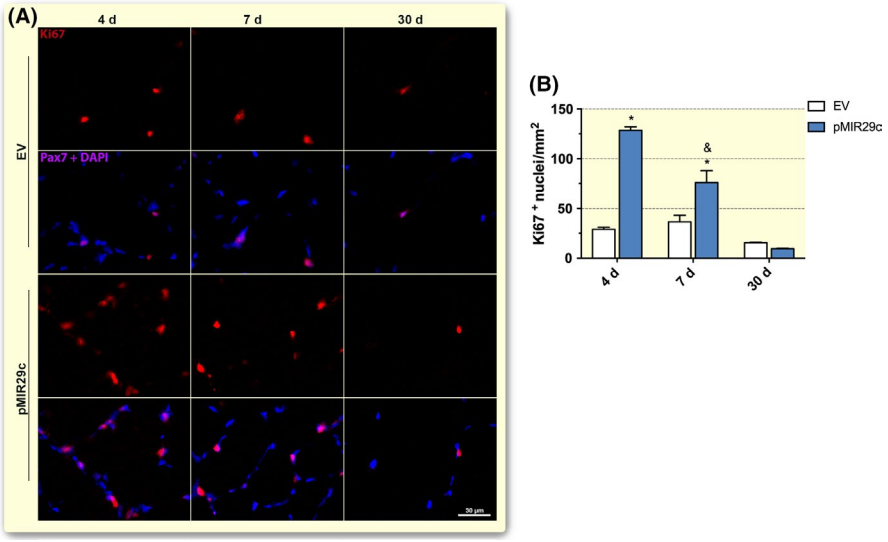

FIGURE 3 miR-29c overexpression increased number of Ki67-positive nuclei in the skeletal muscle. (A) Representative immunofluorescence images of Ki67 in the muscles electrotransfered with EV and pMIR29c vectors for 4, 7 or 30 days. Ki67 (red) and DAPI (blue, used for nuclei identification). (B) Number of positive Ki67 nuclei per mm^2 in EV- and pMIR29c-overexpressing groups; n = 4 per group, scale bar 30 µm. Data are expressed as mean ± SEM. Two-way ANOVA was used to compare the differences between two groups followed by a Bonferroni's post hoc test. $^{*}P < 0.05$ vs EV. $^{\&}P < 0.05$ vs 4 days pMIR29c

single twitch force as compared to that in the control muscles. This pattern was maintained over the entire series of 10 single twitch contractions (Figure 5E), and the specific single twitch force was similar in both groups (Figure 5F). Finally, there was no difference in the T1/2 of the relaxation time or the time-to-peak between the miR-29c-overexpressing and EV muscles (Figure 5G,H).

2.4 | miR-29c regulates the expression of marker genes related to skeletal muscle trophicity

The miR-29c-enhanced skeletal muscle differentiation and hypertrophy suggests that miR-29c may repress the expression and function of genes involved in skeletal muscle trophicity. We therefore monitored the temporal expression pattern of certain hallmark genes related to atrophy (Atrogin-1, MuRF1 and HDCA4) indicated in bold (Table S1), resulting from miR-29c overexpression 4, 7 and 30 days after miR-29c electrotransfer. Atrogin-1 (Fbxo32) and MuRF1 (Trim63) are E3-ligases overexpressed in several models of skeletal muscle atrophy and are therefore known as atrogenes. The inhibition of these genes can also protect the muscle from atrophy.[8] We found reduced mRNA expression levels of MuRF1 at day 4 after electrotransfer (Figure 6A) and reduced protein level at days 4 and 7 after electrotransfer compared to those in the EV group (Figure 6D,E,G,H). Similarly, Atrogin-1 mRNA levels were also downregulated by miR-29c overexpression (Figure 6A,B,D,E,G,H). Histone deacetylase 4 (HDAC4) is related to muscular atrophy induced by denervation and immobilization[30,31] and has been demonstrated to be a direct target of miR-29c.[32] Our results showed that HDAC4 mRNA levels were downregulated by miR-29c at day 7 after electrotransfer (Figure 6B) and protein levels were reduced at days 4 and 7 after electrotransfer compared to those in the EV group (Figure 6D,E,G,H). The mRNA and protein levels of all three genes returned to similar levels as those in the EV group at 30 days after electrotransfer (Figure 6C,F,I).

2.5 | miR-29c promotes differentiation in vitro

The effect of miR-29c in muscle tissue remodelling and functional improvement led us to investigate the changes in the expression of markers of differentiation. We cultured myoblast C2C12 cells and induced differentiation into myotubes for 1, 3 or 5 days and then examined myogenic differentiation. Subsequently, the cells were treated with either miR-29c mimics (or control scramble mimics) or miR-29b (for comparison purposes), and morphometric measurements were performed. The overexpression of miR-29c and miR-29b was confirmed by the increased levels of these miRs at 3 and 5 days after differentiation (Figure 7B,C respectively). Mimic-derived miR-29c overexpression caused a clear increase in myotube diameter (Figure 7A) and eMHC immunostaining at all time points evaluated (~1.6-fold) (Figure 7D,E). Accordingly, miR-29c caused an increased fusion index at all time points evaluated when compared to that in the scramble groups (Figure 7F). Subsequently, we determined the expression levels of the skeletal muscle differentiation

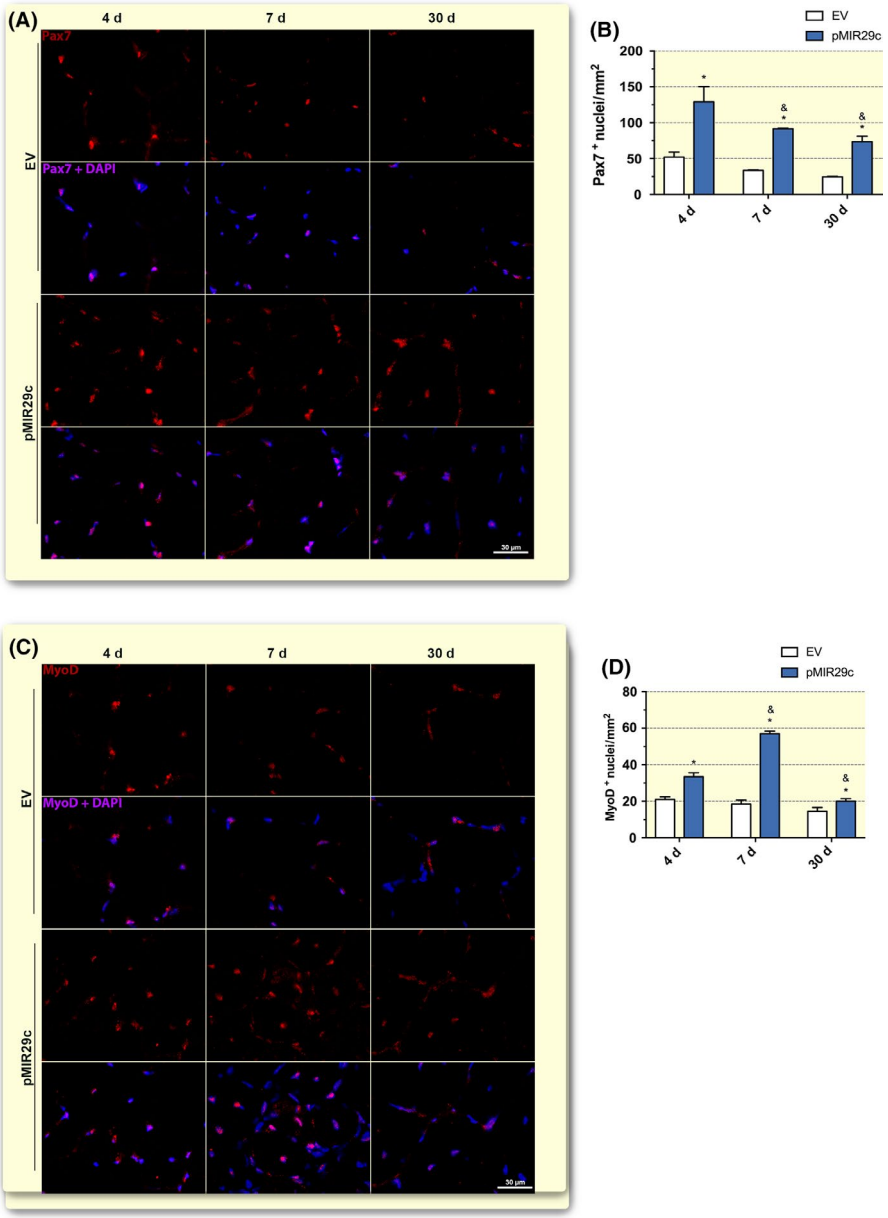

FIGURE 4 miR-29c-overexpressing muscles triggered increased labelling of the myogenic cells markers Pax7 and MyoD. (A) Representative immunofluorescence images of Pax7 (red) and DAPI (blue) in EV and pMIR29c groups in the skeletal muscle sections 4, 7 and 30 days after electrotransfer. (B) Number of positive Pax7 labelling cells per mm^2 in EV and pMIR29c groups. (C) Representative immunofluorescence images of MyoD (red) and DAPI (blue) in EV and pMIR29c groups 4, 7 and 30 days after electrotransfer. (D) Number of positive MyoD cells per mm^2 in EV and pMIR29c groups; n = 4 per group, scale bar 30 µm. Data are expressed as mean ± SEM. Two-way ANOVA was used to compare the differences between two groups followed by a Bonferroni's post hoc test. $^{*}P < 0.05$ vs EV. $^{\&}P < 0.05$ vs 4 days pMIR29c

hallmarks MyoD, MyoG, mMCK and eMHC in C2C12-derived myotubes. miR-29c caused increased expression of MyoD and MyoG after 3 and 5 days of differentiation as compared to that in the control (Figure 7G,H). mMCK and eMHC mRNA levels were also increased by miR-29c after 3 days of differentiation only (Figure 7I,J). Mimic-derived miR-29b overexpression caused a decrease in myofibre size with no alterations in the fusion index level (Figure 7A-F). Additionally, miR-29b overexpression increased MyoD, MyoG, mMCK and eMHC mRNA levels (Figure 7G-J).

2.6 | miR-29c binds directly to the MuRF1 3′UTR

To gain insight into the mechanisms by which miR-29c overexpression can mediate a wide range of pleiotropic effects on skeletal muscle mass and function, we first tested whether miR-29c can inhibit the key atrophy-related E3 ligases Atrogin-1 and MuRF1 and their transcriptional activators FoxO1 and FoxO3 in vitro. Differentiated C2C12 cells exposed to miR-29c showed no difference in FoxO1 mRNA

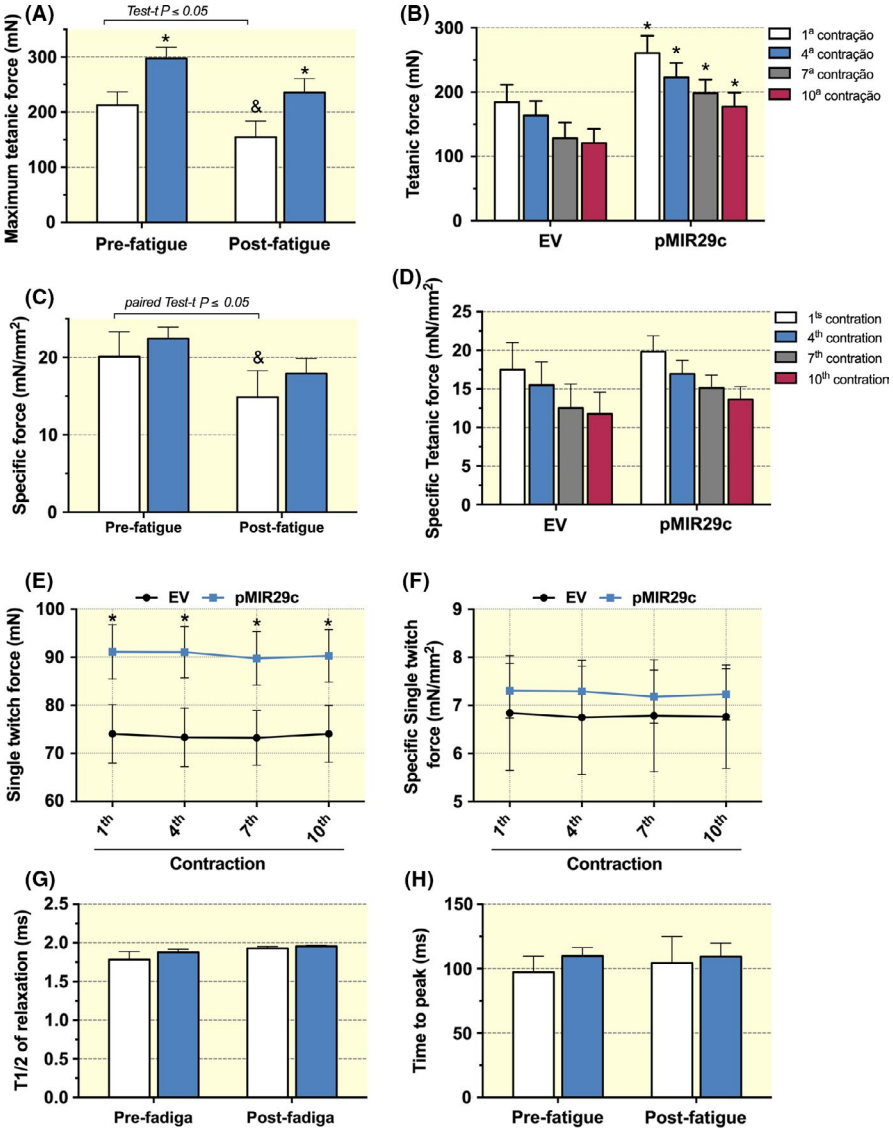

FIGURE 5 Increased contractile measurements in the tibialis anterior overexpressing miR-29c 30 days after electrotransfer. (A) Maximum tetanic force (mN, one contraction at 200 Hz) before (Prefatigue) and after (post-fatigue) the procedure involving a series of 10 contractions at 100 Hz (fatigue protocol). (B) Tetanic force (mN) obtained during the fatigue protocol showing the 1st, 4th, 7th and 10th contraction. (C) Pre- and post-fatigue specific forces and (D) the specific force during the fatigue protocol (mN/mm^2) was determined by maximum tetanic force (mN) divided by the muscle cross-section area (mm^2). (E) A single-twitch force (mN) in EV-pMIR29c groups was obtained at 0.2Hz and specific single-twitch force (F) was determined. (G) Half-relaxation time (ms) and (H) Time to peak (ms) were both obtained by stimulating the muscles at 200 Hz. Data are expressed as mean and SEM; n = 10. $^{*}P \leq 0.05$ vs the respective EV group; $^{\&}P \leq 0.05$ vs prefatigue (analysis of variance followed by Bonferroni's test for multiple comparisons and repeated measures)

levels and a reduction in FoxO3 mRNA levels (after 1 day of differentiation), which paralleled a reduction in MuRF1 mRNA levels at all differentiation time points (Figure 8C). miR-29c caused a complex effect on Atrogin-1 mRNA expression, which was increased after 3 days of differentiation and decreased after 5 days of differentiation (Figure 8D). Mimic-derived miR-29b overexpression caused a decrease in FoxO3 mRNA after 3 days of differentiation, an increase in MuRF1 mRNAs after 3 and 5 days, and an increase in Atrogin-1 mRNA after 5 days of differentiation, compared to the levels in the controls (Figure 8A-D). Because MuRF1 responsiveness to miR-29c was the most intense and widespread over time among the genes evaluated, we decided to examine whether this particular mRNA is a direct target of miR-29c. Atrogin-1 was not chosen because we observed a rather complex response to miR-29c, ie, an elevation after 3 days and a decrease after 5 days of differentiation. Initially, we tested the sensitivity of the MuRF1 3′UTR to miR-29c. For that purpose, we applied increasing doses of a miR-29c mimic (10, 20, 40 (standard dose) and 80 nM) to C2C12 cells 3 days after the onset of differentiation. Although 10 ŋM of miR-29c mimic did not cause a significant drop in MuRF1 mRNA levels, 20, 40 and 80ŋM produced similar levels of downregulation of MuRF1 mRNA (~50%, Figure 8E). To investigate whether the MuRF1 3′UTR is a direct target of miR-29c, we cotransfected C2C12 cells with a miR-29c mimic and a plasmid (pmiRGlo3′UTRMuRF1) containing the MuRF1 3′UTR, which encompass the region between 296 and 302 nt of MuRF1 mRNA (Figure 8F). Subsequently, we determined reporter gene activity (Luciferase). There was a clear decrease in luciferase activity when the miR-29c mimic was transfected into C2C12 cells as compared to the control containing pmiRGlo3′UTRMuRF1-scrambled and also the control containing only pmiRGlo3′UTRMuRF1 (Figure 8G). Accordingly, when the MuRF1 3′UTR was mutated

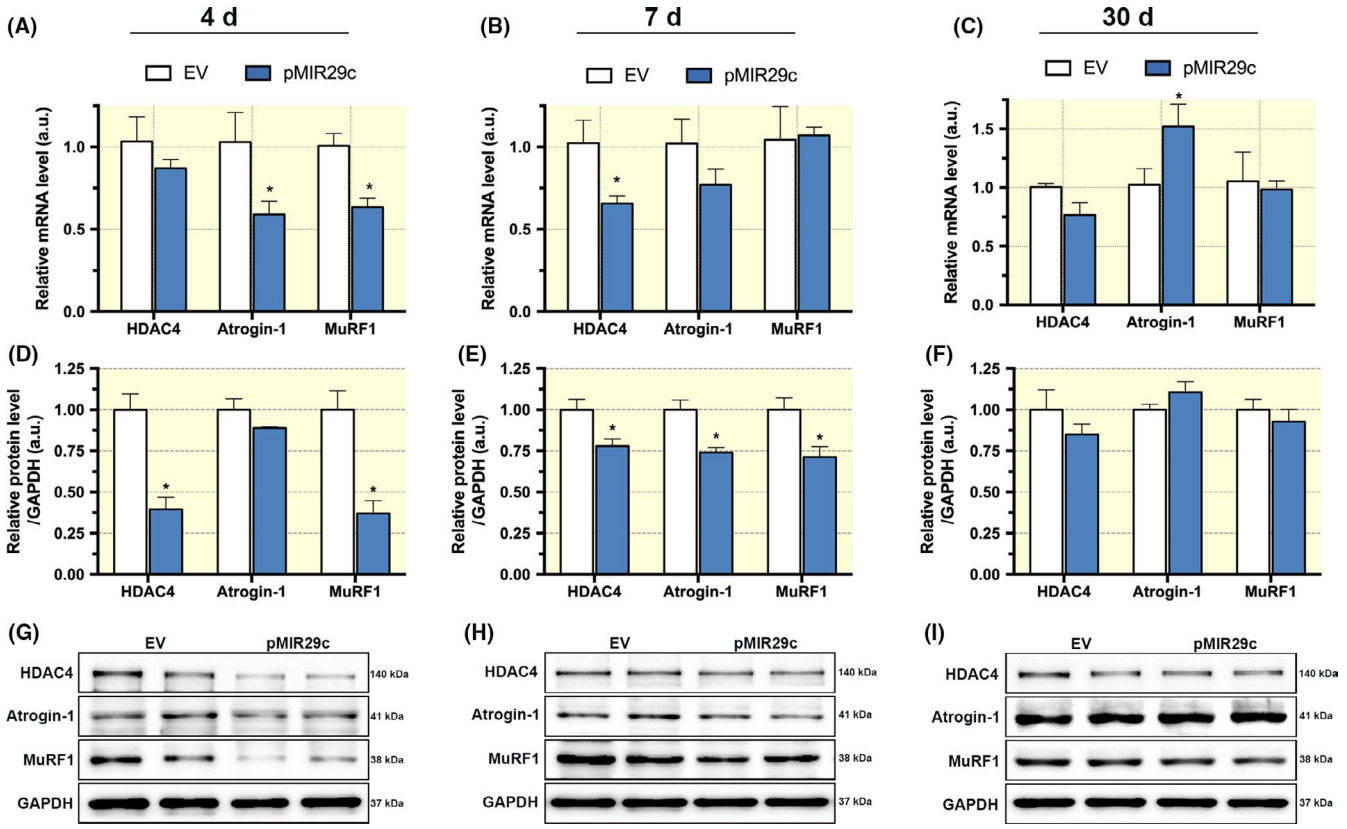

FIGURE 6 miR-29c overexpression modulates gene markers of skeletal muscle trophicity. mRNA levels of MuRF1, Atrogin-1 and HDAC4 were determined by qPCR at 4 (A), 7 (B) and 30 (C) days after electrotransfer in control EV and pMIR29c groups; n = 5 per group. The 18s ribosomal RNA was used as an endogenous control gene. Protein levels of MuRF1, Atrogin-1 and HDAC4 were determined at 4 (D and G), 7 (E and H) or 30 (F and I) days after electrotransfer in control EV and pMIR29c groups. Densitometry (D-F) or representative western blots bands (G-I); n = 5 per group. GAPDH protein level was used as a loading control. Data were expressed in arbitrary units (au) as mean and SEM. Statistical analysis included one-way ANOVA followed by a Tukey's posttest. *$P \leq 0.05$ vs the respective EV group

at the seed site (the point mutations are indicated in red in Figure 8F), the repressive effect of miR-29c mimic was completely abolished, further demonstrating specificity (Figure 8G). To test whether the repressive effect of miR-29c can also occur in other cell systems, we performed the same experiment in HEK293 (Human Embryonic Kidney) cells. The results show a very similar reduction in luciferase activity by miR-29c and the absence of this effect on the mutated MuRF1 3′UTR (Figure 8H). Together, these results indicate that miR-29c directly inhibits the expression of its target MuRF1 by associating with its 3′UTR.

3 | DISCUSSION

In this study, we attempted to identify miRs that regulate skeletal muscle hypertrophy and atrophy, focusing on a combined data mining–experimental approach. We report here that miR-29c drives muscle hypertrophy and myogenic differentiation. The function of miR-29c is, at least in part, mediated by the inhibition of its targets MuRF1 and Atrogin-1, critical regulators of muscle mass. Our initial strategy was focused on searching for miR families (by an in silico approach) that could modulate the genes involved in skeletal muscle mass regulation. The top miR family associated with these mRNAs was miR-340. To our knowledge, there is no report on this miR family acting on skeletal muscle mass regulation, but miR-340 studies are ongoing. In this work, we focused on the miR-29 family, which has already been implicated in myogenesis.

One of the main morphometric findings regarding the muscles overexpressing miR-29c is the increase in the size of the myofibres and the high incidence of split fibres (Figure 2). Split fibres are entities normally found in the muscles subject to extreme overload, as observed in animal models and in humans.[33,34] One prevalent model suggests that, under physiological conditions, upon reaching their maximal size, the fibre can split because the supply of oxygen and exchange of metabolites cannot maintain the diffusion distance.[34] Additionally, under pathological conditions, split fibres are observed in a variety of myopathies, such as muscular dystrophy and Pompe disease.[35,36]

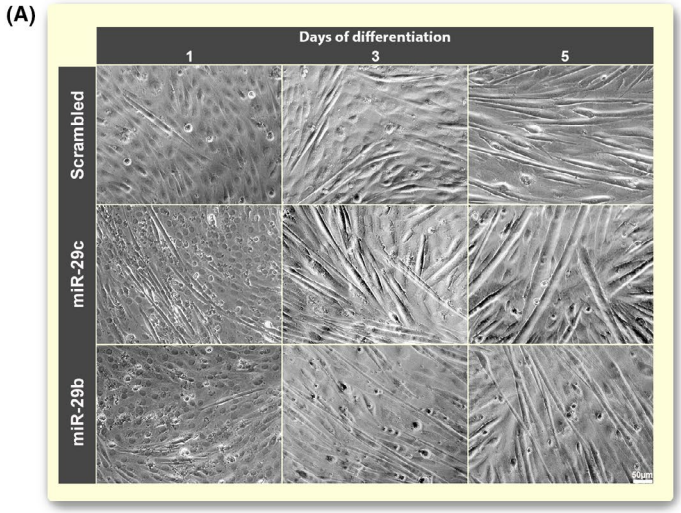
(A)
Days of differentiation
1
3
5
Scrambled
miR-29c
miR-29b
50μm

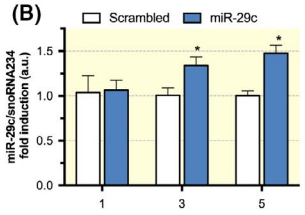
(B)
Scrambled
miR-29c
miR-29c/snoRNA234 fold induction (a.u.)
1.5
1.0
0.5
0.0
1
3
5

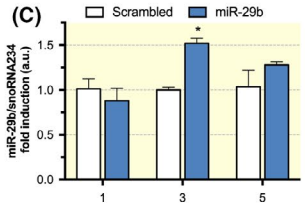
(C)
Scrambled
miR-29b
miR-29b/snoRNA234 fold induction (a.u.)
1.5
1.0
0.5
0.0
1
3
5

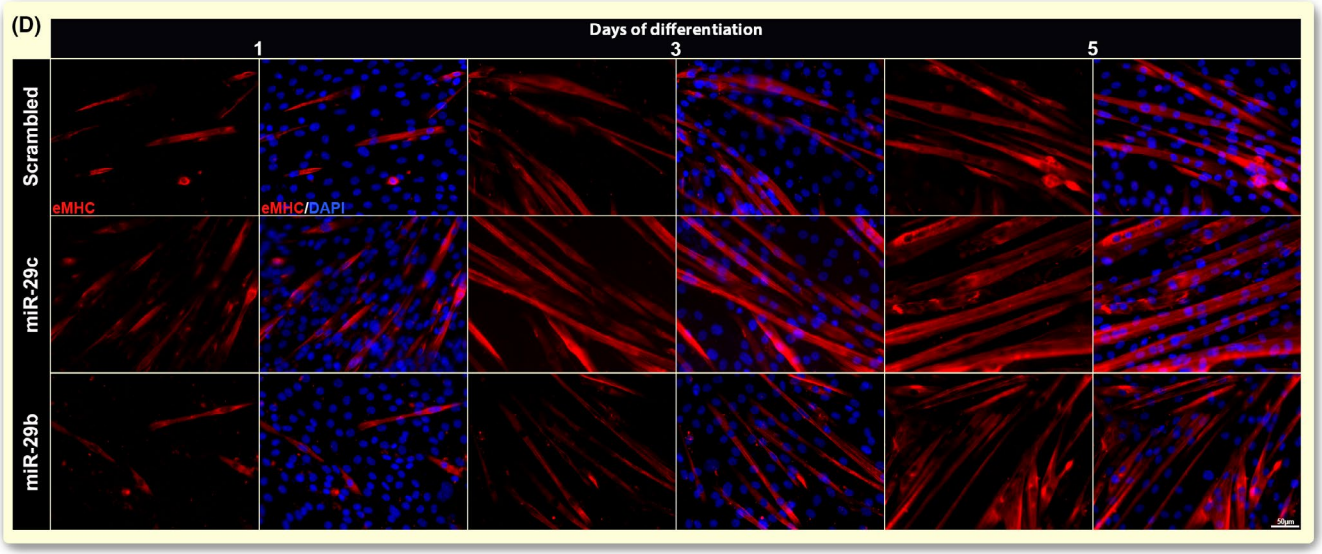
(D)
Days of differentiation
1
3
5
Scrambled
miR-29c
miR-29b
eMHC
eMHC/DAPI
50μm

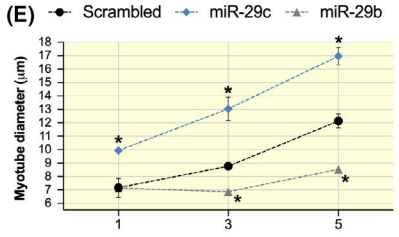
(E)
Scrambled
miR-29c
miR-29b
Myotube diameter (μm)
18
17
16
15
14
13
12
11
10
9
8
7
6
1
3
5

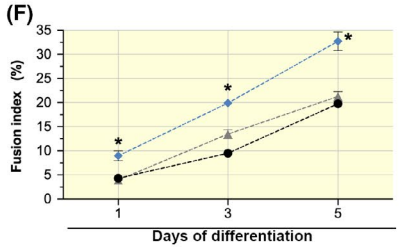
(F)
Fusion index (%)
35
30
25
20
15
10
5
0
1
3
5
Days of differentiation

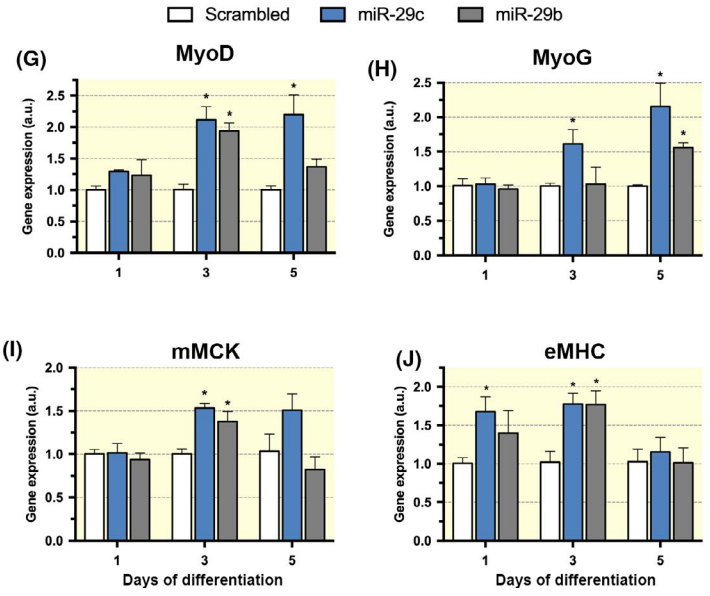
Scrambled
miR-29c
miR-29b
(G)
MyoD
(H)
MyoG
(I)
mMCK
(J)
eMHC
Gene expression (a.u.)
2.5
2.0
1.5
1.0
0.5
0.0
1
3
5
Days of differentiation

FIGURE 7 miR-29c promotes C2C12 differentiation and modulates the mRNA levels of myogenic factors. C2C12 cells were incubated with miR-29c or miR-29b mimics 24 hours before the onset of differentiation and then allowed to differentiate for 1, 3 or 5 days. A scrambled sequence was used as a control. (A) Photomicrographs of representative phase contrast fields 1, 3 and 5 days after differentiation and transfection of each mimic. Scale bar 50 μm. microRNA levels of miR-29c (B) and miR-29b (C) were determined by qPCR. (D) Representative immunofluorescence (eMHC, red) images of myotubes were treated with scrambled and mimic miR29c or miR-29b. Nuclei were stained with DAPI (blue) for nuclei identification. (E) Quantification of myotube diameter and (F) determination of fusion index. For myotube diameter and fusion index measurements, data were expressed as mean ± SEM from two independent experiments; n = 4 per group. Two-way ANOVA was used to compare the differences between two groups followed by a Bonferroni's post hoc test. $*P < 0.05$ vs scrambled group. In these myotubes, the mRNA levels of (G) MyoD, (H) MyoG, (I) mMCK and (J) eMHC were determined. For qPCR of microRNA levels, snoRNA234 was used as an endogenous control gene. For qPCRs, 18s ribosomal RNA was used as an endogenous control gene. For qPCR analysis, data were expressed in arbitrary units (au) as mean and SEM from two independent experiments; n = 4 per group. Statistical analysis included one-way ANOVA followed by a Tukey's posttest. $*P \leq 0.05$ vs scrambled group

In our study, miR-29c-overexpressing muscle showed no signs of inflammatory infiltration (which is normally detected in myopathies) at the microscopy level 30 days after electrotransfer (Figure 2), and we are currently conducting a parallel study to specifically address in detail the cell inflammatory profile in these muscles. Furthermore, miR-29c-overexpressing muscles showed increased length, including a higher number of serial sarcomeres, resulting in longer myofibrils but a sarcomere length still in the range required to generate optimal force (Figure 2G,H). Besides the well-known effect on improving joint range of motion, increased muscle length has been associated with a decreased responsiveness of atrogenes,[37] linking increased muscle length with reduced levels of atrophic pathways. Accordingly, it has been shown that, in humans, stretching sessions can provide protection against injuries caused by a number of sports activities, such as sprinting,[38] soccer[39] and football.[40] In addition, stretching sessions have been shown to increase muscle strength in elderly humans,[41] highlighting the functional importance of increased muscle length.

Overall, these morphological data suggest a beneficial adaptation in the miR-29c-overexpressing muscle. Another morphological characteristic that we observed in the miR-29c-overexpressing muscle is myofibres exhibiting polygonal shapes. This tissue architecture suggests a preserved basal lamina that is typically not found in myopathies, where round fibres predominate. In addition, we have detected high levels of cell proliferation (Figure 3), specifically satellite cells (Figure 4), in miR-29c-overexpressing muscles at early time points after electrotransfer (4 and 7 days), indicating that at the late time point (30 days), the morphometric effects observed are the result of a remodelling at the tissue and cell levels early on (4 days). At the present time, as mentioned earlier, it is not clear whether other cell types, such as inflammatory and other myogenic cells, are also involved in this remodelling phase. Finally, our functional assays clearly show that the miR-29c-overexpressing muscles can generate more force, either at tetanic or single twitch levels, preserving resistance to fatigue and maintaining specific force (Figure 5). These results, along with the findings that of the T½ relaxation time and the time to peak are not altered, indicate that miR-29c-overexpressing muscles generate more force because of mass gain without alterations in calcium handling and intrinsic contractility. Nonetheless, it is important to note that in our experimental set-up miR-29c was transiently expressed. Future studies employing sustained overexpression of miR-29c can help to elucidate the long-term impact of this miR in skeletal muscle.

Another central finding of the present study is the high incidence of centralized nuclei in the miR-29c-overexpressing muscles. It is well accepted that centralized nuclei suggest that the tissue has been previously injured and has undergone the process of regeneration. Additionally, in conditions of continuous cycles of injury and regeneration, such as in dystrophies, centralized nuclei are a predominant feature. On the other hand, the bulk of our data showing increased mass and function suggest that miR-29c overexpression drives a positive adaptive response. As an alternative to the model of injury followed by regeneration, one could envision an independent activation of the myogenic cells, thus driving the fusion of satellite cells to pre-existing fibres and a subsequent increase in size. Indeed, it has been demonstrated that in power-lifting athletes, skeletal muscle fibre size positively correlates with an increased number of centralized nuclei.[42] In the present study, we detected high levels of satellite cell activation 4 days after miR-29c electrotransfer. How miR-29c strongly activates satellite cells is not clear at the moment and will be addressed in a future study. Considering the overall results of this study point to healthy muscle, centralized nuclei may represent an aspect of this positive adaptation.

Further evidence for the positive adaptation of skeletal muscle overexpressing miR-29c comes from the in vitro data of the present study, which reinforces that miR-29c is a potent myogenic inducer. C2C12-derived myotubes transfected with miR-29c are larger than those in control cells (Figure 7), and the mRNA of differentiation markers such as MyoD, MyoG, mMCK and eMHC are increased by miR-29c. This is in line with the intense response that is observable in the

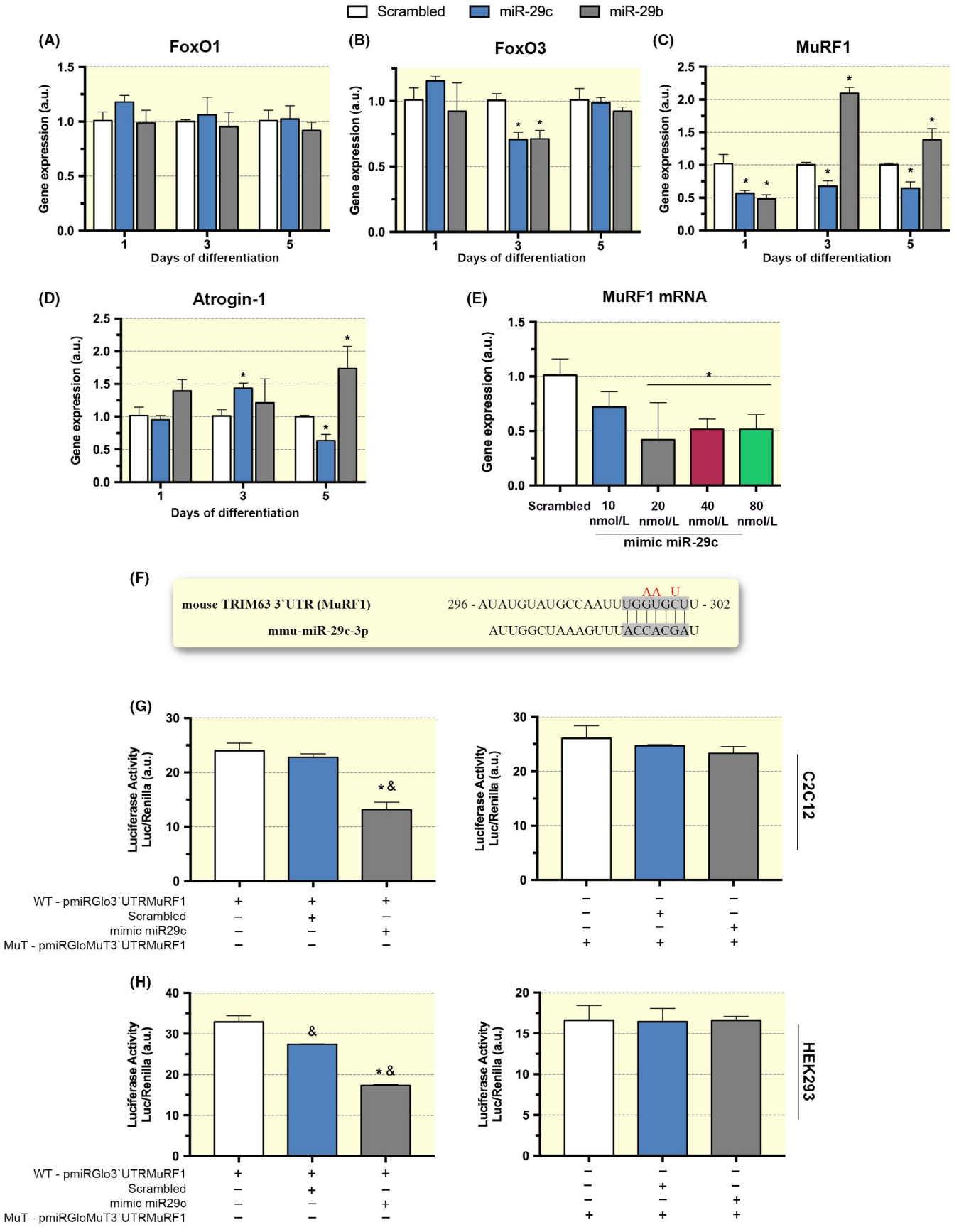
Scrambled
miR-29c
miR-29b
(A)
FoxO1
(B)
FoxO3
(C)
MuRF1
Gene expression (a.u.)
Days of differentiation
(D)
Atrogin-1
(E)
MuRF1 mRNA
Scrambled
10 nmol/L
20 nmol/L
40 nmol/L
80 nmol/L
mimic miR-29c
(F)
mouse TRIM63 3`UTR (MuRF1)
296 - AUAUGUAUGCCAAUUUGGUGCUU - 302
mmu-miR-29c-3p
AUUGGCUAAAGUUUACCACGAU
(G)
Luciferase Activity Luc/Renilla (a.u.)
C2C12
WT - pmiRGlo3`UTRMuRF1
Scrambled
mimic miR29c
MuT - pmiRGloMuT3`UTRMuRF1
(H)
HEK293

FIGURE 8 miR-29c overexpression downregulates the mRNAs related to muscle atrophy by directly binding to the MuRF1 3′ UTR. C2C12 cells were incubated with a miR-29c or miR-29b mimics 24 hours before the onset of differentiation for 1, 3 or 5 days. A scrambled sequence was used as a control. The mRNA levels of (A) FoxO1, (B) FoxO3, (C) MuRF1 and (D) Atrogin-1 were determined by qPCR. Data are expressed in arbitrary units (au) as mean and SEM (n = 4) and normalized to endogenous 18s ribosomal RNA levels. (E) C2C12 cells were treated with a miR-29c mimic at increasing concentrations (10, 20, 40 and 80 ŋM), and MuRF1 mRNA levels were determined by qPCR. $*P \leq 0.05$ vs scrambled group. Statistical analysis included one-way ANOVA followed by a Tukey's posttest. $*P \leq 0.05$ vs scrambled group. (F) Diagram depicting the miR-29c sequence and the 3′ untranslated region (3′UTR) of MuRF1. Seed sequences are highlighted in grey, and the mutations are indicated on the top in red. Luciferase reporter activity driven by the wild-type MuRF1 3′UTR (WT-pmiRGlo3′UTRMuRF1) or a mutated version (MUT-pmiRGlo3′UTRMuRF1) was determined in C2C12 (G) and HEK293 (H) cells. A scrambled sequence was used as a control, and the cells were treated with a miR-29c mimic. Renilla coexpression was used to normalize the transfection. Data were expressed in arbitrary units (au) as mean and SEM; n = 3. $*P \leq 0.05$ vs the scrambled group (blue bars) and $^{\&} P \leq 0.05$ vs vector only group (white bars)

histological data, notably increased fibre size with the incidence of split fibres and myogenesis as indicated by Pax7/MyoD immunolabelling. Because miR-29b has also been implicated in skeletal muscle mass regulation, for comparison purposes, we included this miR in the present study. We have found that a miR-29b mimic caused a reduction in myotube size, in line with a previous study.[22] Additionaly, we have found that miR-29b did not promote changes in the fusion index. Combined, our cell culture experiments indicate that miR-29b is atrophic and that miR-29c is hypertrophic. Intriguingly, both miRs are transcribed in tandem by the same promoter on chromosome 1 in humans, making their antagonistic effects difficult to conciliate at a first glance. Nonetheless, post-transcriptional mechanisms might operate, promoting fine-tune regulation of those particular miRs. For example, it has been recently shown that H19 lncRNA (long non-coding RNA) can act as a miR-29b sponge.[43] This type of mechanism can allow the differential expression of miRs-29b and -29c, conciliating their opposite effects with concomitant transcription.

To further understand the cellular processes that support the pro-trophicity effects of miR-29c overexpression, we evaluated certain potential targets using a time-course approach, which allowed a deeper and more integrated understanding of the tissue response at the molecular level. Both MuRF1 and Atrogin-1 expression were downregulated by miR-29c at 4-7 days after electrotransfer at the mRNA and protein levels, suggesting a prompt response of the expression of the proteins to the decreased mRNA levels (Figure 6). These data are strongly in line with an antiatrophic effect of miR-29c because, in many models of skeletal muscle atrophy (immobilization, tail suspension and denervation), these genes are rapidly upregulated peaking at ~3-5 days and then returning to basal levels.[8] Notably, at 30 days after miR-29c electrotransfer, Atrogin-1 mRNA levels are higher than the controls (Figure 6), which might indicate that the hypertrophic state itself triggers compensatory mechanisms. Interestingly, HDAC4 mRNA levels are still statistically unchanged at 4 days after electrotransfer; nonetheless, protein levels are extremely low (~70% reduction compared to control). At 7 days after electrotransfer, HDAC4 mRNA is decreased with a corresponding decrease in protein levels. We conclude that, in addition to the mechanisms reducing HDAC4 mRNA, other mechanisms involving either the protein translation rate or protein degradation could be operated.

It is initially difficult to conciliate that miR-29c levels are increased 7 days after electrotransfer, and atrophy-related genes are elevated even earlier (4 days after electrotransfer). We interpret this apparent discrepancy over time course as being related to the clearance kinetics of miRs. As soon as the level of a particular miR is elevated, mRNAs start to be targeted, and both the miR and its target mRNAs can be degraded. In fact, it has been described that target RNAs can function as miR sponges.[44] After a particular miR binds to the target mRNA, the mRNA can be degraded along with the miR.[45,46]

MuRF1 is known to be a key molecule in the control of skeletal muscle mass. Mice with a deletion of this gene have muscles resistant to atrophy in models as diverse as denervation (blocked by a mechanical stimulus) and glucocorticoid treatment (by metabolic challenge).[47] Therefore, the link of a mass-modulating agent with decreased MuRF1 levels is particularly significant. Accordingly, in the present study, MuRF1 mRNA was established as a direct target of miR-29c, and in vivo overexpression of miR-29c was shown to drive hypertrophy and decreased the levels of MuRF1 (Figure 6). Finally, in vitro experiments showed that mimic miR-29c induces very large myotubes (Figure 7). Therefore, to get further insight into the molecular mechanisms underlying the effect of miR-29c on MuRF1, we addressed whether the MuRF1 3′UTR is a direct target of this miR. Experiments involving two distinct cell lines confirmed that miR-29c-MuRF1 3′UTR binding is the basis for reduced MuRF1 mRNA levels (Figure 8). MuRF-1 3′UTR is extremely sensitive to miR-29c, and 10nM of a miR-29c mimic (4 times lower than the standard dose) promotes a 25% decrease in MuRF1 mRNA levels (although not statistically significant), and the subsequent doses we tested all produced an ~50% reduction in the level of this mRNA. Therefore, one might envision that slight variations in miR-29c in vivo should produce a major impact on the expression of this mRNA and consequently in muscle mass

levels. We also show here that the seed region of miR-29c is key for the inhibition of MuRF1 mRNA because point mutations in the MuRF1 3′UTR completely abolish this inhibitory effect (Figure 8F-H). Evidently, miR-29c likely binds to the 3′UTR of other mRNAs highlighted in the present study, and further work is necessary to fully address the molecular mechanisms involved in the mass-modulating effects of miR-29c. In the future, it would be highly relevant to directly test the biological impact of miR-29c in models involving atrophy, such as in denervation, glucocorticoid treatment and cachexia.

The miR-29 family has been implicated in many biological processes. It has been shown that miR-29b/c directly binds to the Rybp mRNA, strongly decreasing protein expression.[24] In another study, miR-29a promotes MyoD expression by the direct inhibition of Tet1 mRNA.[27] In addition, miR-29c has been found to be myogenic by directly binding to the 3′UTR of AKT3.[25] These results are in line with the present study, which clearly indicates increased myogenic activity in vivo 4 days after miR-29c electrotransfer, which we envision as being linked to the subsequent hypertrophy observed 30 days after electrotransfer. Remarkably, a recent study revealed that miR-29b overexpression drives increased levels of MuRF1 mRNA and decreased muscle size, the opposite of what we have found with miR-29c. These authors concluded that miR-29b acts on a set of genes to direct skeletal muscle atrophy.[22] Future studies should also address the biological function of miR-29a in skeletal muscle. It is possible that the miR-29 family members play a complex counteractive role in skeletal muscle mass regulation. Other studies have shown that circulatory levels of miR-29a are increased in patients with diabetes.[48] Additionally, Massart et al. showed that miR-29c electrotransfer to the tibialis anterior caused decreased levels of glut4 and AKT expression, suggesting increased insulin resistance. Notably, in those experiments, electrotransfer was performed for 1 week.[49] In our experiments, we did not observe any increase in skeletal muscle mass 1 week after miR-29c electrotransfer; rather, we observed intense myogenesis, which might be related to a transient depression of the insulin pathway. Certainly, future studies are needed to further clarify the role of the individual members of the miR-29 family in skeletal muscle plasticity, ie, myogenesis, skeletal muscle mass, insulin activity and other reported effects such as antifibrosis, tumour suppression and antiviral activity.[50-52]

In conclusion, miR-29c drives a skeletal muscle response, leading to increased mass and a gain of function, highlighting that this miR might be useful as a future therapeutic tool to manipulate skeletal muscle mass in clinical settings, miRs represent a unique therapeutic approach to fight disease because one single miR can target multiple mRNAs, thereby reaching different pathways. In fact, several pharmaceutical companies have invested efforts to develop miR-based therapies either to overexpress a chosen miR or to inhibit it via specific nucleic acid sequences named locked nucleic acid (LNA) inhibitors.[53] It has been recently reported that a miR-122 LNA inhibitor can block hepatitis C viral replication in clinical trials.[54] In addition, overexpression of miR-486 has been employed in animal models of Duchenne muscular dystrophy, in which it was shown to alleviate disease progression via DOCK3 inhibition.[55] Therefore, it seems likely that miR-based therapies will soon be present in the clinical setting. For skeletal muscle, miR-29c might represent an attractive entry point for treating skeletal muscle deficits in the skeletal muscle diseases where a combined improvement for trophicity and function would be beneficial.

4 | MATERIALS AND METHODS

The experimental procedures used in this study conform to the Brazilian College of Animal Experimentation (approved by the Institute of Biomedical Sciences animal experimentation office #168/05).

Adult male C57BL/6 mice (8-12 weeks old, 24.9 ± 1.1g) were kept in standard cages with controlled temperature and allowed free access to standard food and water. The animals were maintained at an animal house at the Institute of Biomedical Sciences, USP.

Mice were killed by cervical dislocation and immediately TA muscles were removed, weighed, transversally cut into two halves, frozen in hyper-cooled isopentane and then stored in liquid nitrogen for subsequent analysis. One half was used to Hematoxylin and Eosin (H/E) staining and immunofluorescence. The other half was used for gene analysis.

4.1 | In vivo muscle transfection by electric field (electrotransfer)

In vivo experiments involving transfection of miR-29c expression vector were conducted on 8-week-old mice tibialis anterior (TA), which were submitted to a small incision in the skin to apply five injections (5 µl, 40U) of Hyaluronidase (Sigma #H3506, Germany). After 30 minutes, the muscles received four injections (5 µL each) of a miR-29c expression vector (2.5 µg/µL, pCMVmiR-29c, Origen, USA) sideways the long axis of the muscle or the empty vector (EV) pCMV-MIR. Subsequently, platinum-made electrodes (3 mm wide, 7 mm long) were placed in parallel in opposite sides of the muscle along its long axis and a burst of pulses was delivered (5 pulses of 20 ms with 980 ms pause, 50 V, 5 mm distance between electrodes) by an electric pulse generator (constructed and calibrated by the Institute of Nuclear Research, Brazil).

4.2 | Plasmid constructions

The 3′-UTR of mouse Trim63 (MuRF1) with the region of miR-29c binding site was PCR amplified using the following primers 5′-AAAGCTAGCATGAGTGAGACACGCTCTGGA-3′ with NheI fragment and 5′-AAATCTAGAAGGCAGAGTCT CTCTATGTAGCTC-3′ with XbaI fragment, and cloned into the pmiRGlo (Promega). The construct was sequenced and named WT-pmiRGlo3′UTRMuRF1. The predicted miR-29c binding site located in the MuRF1 3′UTR was mutated using a PCR-based mutagenesis strategy with combinations of the primers above and the following oligo 5′-TGCCAATTTGAAGTTTTTTGTACGAGAAC-3′, as per the protocol by Q5® Site-Directed Mutagenesis Kit (NEB). The construct was sequenced, to confirm the mutated site (underlined) and named MUT-pmiRGlo3′UTRMuRF. The Renilla Luciferase in the pmiRGlo plasmid (Promega) was used as a control to normalization loading in the luciferase assays. The plasmids pMIR29c and EV (pCMVMIR) were purchased from OriGene Technologies (PCMVMIR) and contains Green Fluorescence Protein (GFP) as a reporter to monitor the gene delivery in the electrotransfer experiments.

4.3 | Cells transfection and luciferase assay

Mouse C2C12 myoblasts were plated at a density of 80% confluence in wells (~11 mm^2) with proliferation medium (DMEM, 10% FBS and 1% Penicillin and Streptomycin (P/S); Invitrogen, Carlsbad, CA, USA). Subsequently, cells were transfected with 40 nM, miR-29b, miR-29c mimics or negative Control#1 as a Scrambled sequence (Ambion Inc, USA) using Lipofectamine 2000 (LF2000; Invitrogen, USA), following manufacturer's instructions. After 24 hours, the medium was changed and cells were induced to differentiation (DMEM, 2% HS and 1% P/S; Invitrogen, Carlsbad, CA, USA). After 1, 3 or 5 days, the cells were harvested and the RNA were isolated as stated above protocol.

To achieve myotube fusion index measurements, six immunofluorescence images (eMHC labelling) per sample were chosen randomly (~1 mm^2). Subsequently, the number of nuclei inside eMHC-positive cells and the total number of total nuclei (DAPI) were counted. Then the percentage of nuclei within myotubes was calculated.

To perform luciferase assays, HEK293 and C2C12 cells were seeded at a density of 80% confluence in 24-well plates in proliferation medium. Subsequently, mimic miR-29c or Scrambled were co-transfected with WT-pmiRGlo3′UTR-MuRF1 or MUT-pmiRGlo3′UTRMuRF1 plasmids (500ng of each). After 24 hours, cells were harvested and a luciferase assay was performed following the Dual-Luciferase® Reporter Assay System (Promega).

4.4 | In silico analysis

First, we selected in the literature a set of studied and recognized genes, involved in the regulation of muscle mass control. We selected 65 genes linked to muscle mass regulation in a protrophicity (27 genes) or proatrophy (38 genes) manner. Next, we used the TargetScan database (www.targetscan.org) to identified putative regulatory miRs that predicted these genes as a target which were conserved between mouse, rat and humans. The miRs were rated based on the number of mRNA hits obtained (minimum of six hits were considered for rating) and only relations with $P_{CT} > 0$ were considered. Finally, the hits were counted and the miRs were sorted according to mRNA count. Detailed information regarding the prediction algorithm, parameter settings and raw data source is available on the above link. Details for choosing miR-29c is presented in the results section.

4.5 | RNA extraction

Muscle samples (25 mg) were homogenized using a Polytron© and total RNA was isolated with Trizol (Invitrogen©) according to the guidelines. The samples were dissolved in ultra-pure water, and their concentrations were determined by absorbance at 260 nm with a spectrophotometer (Eppendorf©). The pureness of the RNA was confirmed by establishing the ratio between measurements at 260 and 280 nm and RNA integrity was checked on a denaturant 1% agarose ethidium bromide stained gel.

4.6 | Quantitative real-time polymerase chain reactions (qPCR)

For miR expression analysis, 10 ng of the total RNA was used in a cDNA reaction containing 5X Loop Primers for RT-PCR specific for each miRNA that was analysed, 100nM dNTP mix with dTTP, 10X RT buffer, RNase inhibitor (20U/ul), nuclease free water and 50 units of MultiScribe™ RT enzyme (TaqMan® microRNA RT Kit—B™) performed at 16ºC for 30 minutes followed by 42ºC for 30 and 5 minutes at 85ºC. One microlitre of cDNA was used in real-time PCR, containing TaqMan® Universal Master Mix II (AB™), TaqMan® MGB probes specific for the analysed miR (TaqMan® microRNA Assays—AB™ cat#4427975) and nuclease-free water. Cycle parameters were 50°C for 2 minutes, 95°C for 10 minutes, followed by 40 cycles of 95°C for 15 seconds, and 60°C for 1 minute. Fluorescence intensity was quantified with a qPCR thermocycler (Corbett RotorGene 6000, Qiagen©).

For gene expression analysis, 1 µg of total RNA was used in the cDNA reaction and 1 µl of this was used to perform the real-time PCR, containing Eva Green qPCR supermix (Solis Biodyne©), 200 nM of each primer,

forward and reverse (complete list of primers in Table S3) and nuclease-free water. Cycle parameters were 95°C for 12 minutes, followed by 40 cycles of 95°C for 15 seconds, 60°C for 30 seconds and 72°C for 30 seconds. The 18S ribosomal RNA was used as an internal control. Detailed cDNA reactions and result analysis were followed as described elsewhere.[56]

4.7 | Western-blot analysis

A chilled mortar with liquid nitrogen was used to grind a small piece of TA muscle into a fine powder. Then, homogenized in RIPA buffer (1 mM EDTA, pH 7.4, 0.0625% sodium deoxycholate, 0.0625% nonidet P-40, 6.2 mM sodium phosphate and 1x Halt protease and phosphatase inhibitor cocktail—Thermo Scientific cat#78445). Homogenates were incubated on ice for 10 minutes, centrifuged at 10.000 g for 10 minutes at 4°C after the supernatant containing the total protein was stored at −80°C.

Protein concentration was determined by the Bradford method[57] with bovine serum albumin (BSA) as standard. Equal amounts of total protein (5-30 μg) were loaded on to a 12% SDS:acrylamide gel (SDS-PAGE) and separated by electrophoresis. Proteins were transferred to a nitrocellulose membrane in a semi-dry system. The membranes were then stained with Ponceau to confirm equal loading and also the quality of protein extracts. All membranes were incubated with 5% non-fat milk in Tris-buffered saline with Tween (0.5 M NaCl, 50 mM Tris-HCl pH 7.4, 0.1% Tween 20) for 50 minutes. Then, membranes were washed three times for 5 minutes each with Tris-buffered saline with Tween and incubated with primary antibody with 5% BSA in Tris-buffered saline with Tween. The following primary antibodies were used: rabbit anti-HDAC4 (1:1000, cat#7628, Cell Signaling); rabbit anti-Atrogin-1 (1:1000, cat#AP2041, ECM Biosciences); rabbit anti-MuRF1 (1:1000, cat#MP3401, ECM Biosciences).

After primary antibody incubation, membranes were incubated with a secondary antibody (1:10.000, goat anti-rabbit peroxidase cat#111035003, Jackson ImmunoResearch) with 5% BSA in Tris-buffered saline with Tween for 1 hour at room temperature. Subsequently, the membranes were washed three times for 5 minutes each with Tris-buffered saline and Tween. Specific bands were visualized by Luminata™ Forte (cat#WBLUF0500, Millipore) in the Fusion FX5 XT (Vilber Lourmat). Loading variations were monitored by GAPDH endogenous control, and densitometry of the protein bands were determined in the imageJ software (v. 1.45s, National Institutes of Health).

4.8 | Cross-sectional area

Mice were killed, and TA muscles were removed, snap-frozen in isopentane and kept in liquid nitrogen. Subsequently, the muscles were transversely sectioned (10-μm-thick) by employing a cryostat (Leica CM1850 UV, Wetzlar, Germany) and subsequently stained with hematoxylin-eosin. The CSA of muscle fibres was determined with the ImageJ software (v. 1.45s, National Institutes of Health). About 300 fibres per muscle were analysed using the microscope Axio Scope.A1 (Carl Zeiss Microscopy GmbH, Göttingen, Germany).

4.9 | Immunofluorescence

Muscle cross-section was fixed with 4% PFA at room temperature for 10 minutes, washed (2 times for 3 minutes each) with PBS-T (PBS with 0.1% Tween 20) and incubated for 1 hour with blocking solution (1% bovine serum albumin in PBS-T). The membranes were then incubated overnight at 4ºC with primary antibody rabbit anti-eMHC (1:500, Origene cat#TA349138), rabbit anti-GFP (1:250, Invitrogen cat#A10260), rabbit anti-Ki67 (1:200, Cell Signaling cat#9129), rabbit anti-Pax7 (1:50, Abcam cat#ab34360) or rabbit anti-MyoD (1:50, Santa Cruz cat# sc-304). After washing with PBS-T 0.1% (3 times for 5 minutes each), secondary antibody (1:250 Cy3 Donkey Anti-Rabbit or Cy2 Donkey Anti-Rabbit, both Jackson ImmunoResearch) was added in blocking solution for 1 hour in the dark, followed by further washing three times for 5 minutes in PBS-T. Finally, slides were mounted with coverslips with Vectashield for fluorescence with 4′,6-diamidino-2-phenylindole (DAPI) (cat# H-1200, Vector Labs). Digital capture of the stained sections was performed with a fluorescence microscope Axio Scope. A1 (Carl Zeiss Microscopy GmbH, Göttingen, Germany).

4.10 | Muscle function experiments in vivo

Function analysis of skeletal muscle was performed as previously described.[58] We have used Tribromoethanol (20 mg/100 g of body wt, ip) to anaesthetize animals, which was followed by a lateral incision to expose the sciatic nerve and an electrode was connected. Animals were immobilized in acrylic platform and the TA tendon was coupled to a force transducer that was employed to analyse data regarding the strength and muscle contraction. At the onset of experiments, the muscles were set to the optimum length (defined as the length providing the maximum twitch force). Maximum tetanic force, tetanic force and single twitch force were recorded using a data acquisition and analysis system (Aqda, Ancad, São Carlos, Brazil). To measure the maximum tetanic force, a 200-Hz stimuli protocol was applied to reach maximal plateau using minimal frequency and 100 Hz to evaluate fatigue. Single twitches (0.2 Hz) were generated for 2 minutes, followed by a 2-second pre-fatigue maximum tetanic contraction (at 200 Hz).[59] Subsequently, a fatigue protocol was performed (ten 2-second stimulations at 100 Hz tetanus) each followed by a 4-second rest.

Then, a 2-minute rest period was allowed to the muscle by stimulation at 0.2 Hz. Then, a post-fatigue maximum tetanic contraction protocol was performed. In maximum tetanic force protocols, the time-to-peak and half-relaxation time parameters were available. The muscle force decline was determined at 1st, 4th, 7th and 10th contraction. Maximum tetanic force, tetanic force and isolated twitches were expressed in millinewtons and specific force was determined by the maximum tetanic force/CSA ratio, expressed in milinewtons/mm^2. Specific force was determined by dividing measurements of force by muscle CSA.

4.11 | Determination of sarcomeres in series

The muscle fixation and fibre isolation procedures were adapted as described by other authors.[60] Mice were killed by cervical dislocation and TA muscles were exposed and fixed in situ by pipetting a fixative solution (2.5% glutaraldehyde pH 7-5, 0.1 M phosphate buffer and 0.5% glucose) for 20 minutes. Then, entire hind limb was removed and placed in the fixative solution with the ankle joint angle at 90°. After 1 hour, the TA muscles were dissected out, placed in fresh fixative solution for 90 minutes, followed a wash with fresh fixative solution. Subsequently, using a Vernier caliper, the distance between the muscle-tendon junctions was measured. Thereafter, to dissociate connective tissue, the muscles were placed in 30% (w/v) HNO for 2 days, followed by a wash with phosphate-buffered saline (PBS) and stored in 50% glycerol. To isolate the fibres in a dissecting microscope, we used an electrolytically sharpened tungsten needles to tease out individual whole fibres.[60] After, six fibres from each muscle were randomly chosen and are positioned horizontally on a glass sheet and mounted with glycerol jelly and coverslips to avoid the compression of the fibers. Digital acquisitions of the fibres were obtained with a light microscope (Zeiss Imager M1) and the number of sarcomeres in series was measured within 300 μm per fibre (n = 4).

4.12 | Statistical analysis

Data are presented as mean ± SEM. Multiple comparisons were established using either one-way ANOVA and the Student-Newman-Keuls post hoc test or two-way ANOVA and the Bonferroni's post hoc test. The unpaired *t* test was employed to compare the differences between two groups and the paired *t* test to compare the differences into a group. All analyses were accomplished by GraphPad Prism 6.0. For comparisons, a $P < 0.05$ was considered as significant.

ACKNOWLEDGEMENTS

This study was funded by grant: #2012/07018-0, #2012/22488-2 and #2015/04090-0 Sao Paulo Research Foundation (FAPESP); National Council for Scientific and Technological Development (CNPq); the European Union for financial support (Horizon 2020 research and innovation programme grant agreement No 645648 Muscle Stress Relief), and the Leducq Foundation, network 13CVD04. Research in the Wang lab was supported by grants HL085635 and HL116919 (NIH, USA).

CONFLICTS OF INTEREST

Anselmo Moriscot and William Silva have a related patent pending BR 10 2018 067702 0. The submitted material is conform with Good Publishing Practice in Physiology: Good publication practice in physiology: Acta Physiol (Oxf). 2017 Dec;221(4):283-284.

ORCID

William José Silva https://orcid.org/0000-0001-6969-3464
André Cruz https://orcid.org/0000-0001-7977-8752

REFERENCES

1. Janssen I, Heymsfield SB, Wang Z, Ross R. Skeletal muscle mass and distribution in 468 men and women aged 18–88 yr. *J Appl Physiol*. 2017;89:81-88. https://doi.org/10.1152/jappl.2000.89.1.81.
2. Gransee HM, Mantilla CB, Sieck GC. Respiratory muscle plasticity. *Compr Physiol*. 2012;2:1441-1462.
3. Schiaffino S, Dyar KA, Ciciliot S, Blaauw B, Sandri M. Mechanisms regulating skeletal muscle growth and atrophy. *FEBS J*. 2013;280:4294-4314.
4. Lecker SH, Solomon V, Mitch WE, Goldberg AL. Muscle protein breakdown and the critical role of the ubiquitin-proteasome pathway in normal and disease states. *J Nutr*. 1999;129(1S Suppl):227S-237S. https://doi.org/10.1093/jn/129.1.227S.
5. Sandri M. Protein breakdown in muscle wasting: Role of autophagy-lysosome and ubiquitin-proteasome. *Int J Biochem Cell Biol*. 2013;45(10):2121-2129. https://doi.org/10.1016/j.biocel.2013.04.023.
6. Schakman O, Kalista S, Barbé C, Loumaye A, Thissen JP. Glucocorticoid-induced skeletal muscle atrophy. *Int J Biochem Cell Biol*. 2013;45(10):2163-2172. https://doi.org/10.1016/j.biocel.2013.05.036.
7. Londhe P, Guttridge DC. Inflammation induced loss of skeletal muscle. *Bone*. 2015;80:131-142. https://doi.org/10.1016/j.bone.2015.03.015.
8. Bodine SC, Latres E, Baumhueter S, et al. Identification of ubiquitin ligases required for skeletal muscle atrophy. *Science(80-)*. 2001;294(5547):1704-1708. https://doi.org/10.17531/ein.2016.1.6.
9. Gomes MD, Lecker SH, Jagoe RT, Navon A, Goldberg AL. Atrogin-1, a muscle-specific F-box protein highly expressed during muscle atrophy. *Proc Natl Acad Sci U S A*. 2001;98:14440-14445.
10. Rommel C, Bodine SC, Clarke BA, et al. Mediation of IGF-1-induced skeletal myotube hypertrophy by Pl(3)K/Alt/mTOR and

Pl(3)K/Akt/GSK3 pathways. *Nat Cell Biol*. 2001;3(11):1009-1013. https://doi.org/10.1038/ncb1101-1009.
11. Schuelke M, Wagner KR, Stolz LE, et al. Myostatin mutation associated with gross muscle hypertrophy in a child. *N Engl J Med*. 2004;350(26):2682-2688. https://doi.org/10.1056/NEJMoa040933.
12. Hammers DW, Merscham-Banda M, Hsiao JY, Engst S, Hartman JJ, Sweeney HL. Supraphysiological levels of GDF11 induce striated muscle atrophy. *EMBO Mol Med*. 2017;9:531-544.
13. Nie M, Deng Z-L, Liu J, Wang D-Z. Noncoding RNAs, emerging regulators of skeletal muscle development and diseases. *Biomed Res Int*. 2015;2015:676575.
14. Chen J-F, Callis TE, Wang D-Z. microRNAs and muscle disorders. *J Cell Sci*. 2009;122:13-20.
15. Desvignes T, Batzel P, Berezikov E, et al. MiRNA Nomenclature: a view incorporating genetic origins, biosynthetic pathways, and sequence variants. *Trends Genet*. 2015;31(11):613-626. https://doi.org/10.1016/j.tig.2015.09.002.
16. van Rooij E, Liu N, Olson EN. MicroRNAs flex their muscles. *Trends Genet*. 2008;24:159-166.
17. Sweetman D, Goljanek K, Rathjen T, et al. Specific requirements of MRFs for the expression of muscle specific microRNAs, miR-1, miR-206 and miR-133. *Dev Biol*. 2008;321:491-499.
18. McCarthy JJ. MicroRNA-206: the skeletal muscle-specific myomiR. *Biochim Biophys Acta*. 2008;1779:682-691.
19. Wada S, Kato Y, Okutsu M, et al. Translational suppression of atrophic regulators by MicroRNA-23a integrates resistance to skeletal muscle atrophy. *J Biol Chem*. 2011;286:38456-38465.
20. McFarlane C, Vajjala A, Arigela H, et al. Negative auto-regulation of myostatin expression is mediated by Smad3 and MicroRNA-27. *PLoS ONE*. 2014;9(1):e87687. https://doi.org/10.1371/journal.pone.0087687.
21. Wang H, Garzon R, Sun H, et al. NF-κB-YY1-miR-29 regulatory circuitry in skeletal myogenesis and rhabdomyosarcoma. *Cancer Cell*. 2008;14:369-381.
22. Li J, Chan MC, Yu Y, et al. MiR-29b contributes to multiple types of muscle atrophy. *Nat Commun*. 2017;8:1-15.
23. Kriegel AJ, Liu Y, Fang Y, Ding X, Liang M. The miR-29 family: genomics, cell biology, and relevance to renal and cardiovascular injury. *Physiol Genomics*. 2012;44:237-244.
24. Zhou L, Wang L, Lu L, Jiang P, Sun H, Wang H. A novel target of microRNA-29, Ring1 and YY1-binding protein (Rybp), negatively regulates skeletal myogenesis. *J Biol Chem*. 2012;287:25255-25265.
25. Wei W, He H-B, Zhang W-Y, et al. miR-29 targets Akt3 to reduce proliferation and facilitate differentiation of myoblasts in skeletal muscle development. *Cell Death Dis*. 2013;4:e668.
26. Wang XH, Hu Z, Klein JD, Zhang L, Fang F, Mitch WE. Decreased miR-29 suppresses myogenesis in CKD. *J Am Soc Nephrol*. 2011;22:2068-2076.
27. Chikenji A, Ando H, Nariyama M, Suga T, Iida R, Gomi K. MyoD is regulated by the miR-29a-Tet1 pathway in C2C12 myoblast cells. *J Oral Sci*. 2016;58:219-229.
28. Scholzen T, Gerdes J. The Ki-67 protein: From the known and the unknown. *J Cell Physiol*. 2000;182(3):311-322. https://doi.org/10.1002/(SICI)1097-4652(200003)182:3<311:AID-JCP1>3.0.CO;2-9.
29. Musarò A. The basis of muscle regeneration. *Adv Biol*. 2014;2014:1-16. https://doi.org/10.1155/2014/612471.
30. Bongers KS, Fox DK, Ebert SM, et al. Skeletal muscle denervation causes skeletal muscle atrophy through a pathway that involves both Gadd45a and HDAC4. *AJP Endocrinol Metab*. 2013;305(7):E907-E915. https://doi.org/10.1152/ajpendo.00380.2013.
31. Yoshihara T, Machida S, Kurosaka Y, Kakigi R, Sugiura T, Naito H. Immobilization induces nuclear accumulation of HDAC4 in rat skeletal muscle. *J Physiol Sci*. 2016;66(4):337-343. https://doi.org/10.1007/s12576-015-0432-1.
32. Winbanks CE, Wang B, Beyer C, et al. TGF-β regulates miR-206 and miR-29 to control myogenic differentiation through regulation of HDAC4. *J Biol Chem*. 2011;286:13805-13814.
33. Antonio J, Gonyea WJ. Skeletal muscle fiber hyperplasia. *Med Sci Sports Exerc*. 1993;25:1333-1345.
34. Eriksson A, Lindström M, Carlsson L, Thornell LE. Hypertrophic muscle fibers with fissures in power-lifters; fiber splitting or defect regeneration? *Histochem Cell Biol*. 2006;126:409-417.
35. Head SI, Williams DA, Stephenson DG. Abnormalities in structure and function of limb skeletal muscle fibres of dystrophic mdx mice. *Proc R Soc B Biol Sci*. 1992;248(1322):163-169. https://doi.org/10.1098/rspb.1992.0058.
36. Lagalice L, Pichon J, Gougeon E, et al. Satellite cells fail to contribute to muscle repair but are functional in Pompe disease (glycogenosis type II). *Acta Neuropathol Commun*. 2018;6(1):116. https://doi.org/10.1186/s40478-018-0609-y.
37. Soares AG, Aoki MS, Miyabara EH, et al. Ubiquitin-ligase and deubiquitinating gene expression in stretched rat skeletal muscle. *Muscle Nerve*. 2007;36:685-693.
38. Sugiura Y, Sakuma K, Sakuraba K, Sato Y. Prevention of hamstring injuries in collegiate sprinters. *Orthop J Sport Med*. 2017;5(1). https://doi.org/10.1177/2325967116681524.
39. Arnason A, Andersen TE, Holme I, Engebretsen L, Bahr R. Prevention of hamstring strains in elite soccer: an intervention study. *Scand J Med Sci Sport*. 2008;18(1):40-48. https://doi.org/10.1111/j.1600-0838.2006.00634.x.
40. Verroll GM, Slavotinek JP, Barnes PG. The effect of sports specific training on reducing the incidence of hamstring injuries in professional Australian rules football players. *Br J Sports Med*. 2005;39(6):363-368. https://doi.org/10.1136/bjsm.2005.018697.
41. Inami T. Long-term Stretching Program in Older Active Adults Increases Muscle Strength. *J Exerc Sport Orthop*. 2014;1. https://doi.org/10.15226/2374-6904/1/2/00112.
42. MacDougall JD, Sale DG, Elder GCB, Sutton JR. Muscle ultrastructural characteristics of elite powerlifters and bodybuilders. *Eur J Appl Physiol Occup Physiol*. 1982;48(1):117-126. https://doi.org/10.1007/BF00421171.
43. Lu YF, Liu Y, Fu WM, et al. Long noncoding RNA H19 accelerates tenogenic differentiation & promotes tendon healing through targeting miR-29b-3p & activating TGF-β1 signaling. *FASEB J*. 2017;31(3):954-964. https://doi.org/10.1096/fj.201600722R.
44. Thomson DW, Dinger ME. Endogenous microRNA sponges: evidence and controversy. *Nat Rev Genet*. 2016;17(5):272-283. https://doi.org/10.1038/nrg.2016.20.
45. Rüegger S, Großhans H. MicroRNA turnover: when, how, and why. *Trends Biochem Sci*. 2012;37(10):436-446. https://doi.org/10.1016/j.tibs.2012.07.002.
46. Ghini F, Rubolino C, Climent M, Simeone I, Marzi MJ, Nicassio F. Endogenous transcripts control miRNA levels and activity in mammalian cells by target-directed miRNA degradation. *Nat Commun*. 2018;9(1):3119. https://doi.org/10.1038/s41467-018-05182-9.

47. Baehr LM, Furlow JD, Bodine SC. Muscle sparing in muscle RING finger 1 null mice: response to synthetic glucocorticoids. *J Physiol*. 2011;589:4759-4776.
48. Kong L, Zhu J, Han W, Jiang X, Xu M, Zhao Y, et al. Significance of serum microRNAs in pre-diabetes and newly diagnosed type 2 diabetes: a clinical study. *Acta Diabetol*. 2011;48:61-69.
49. Massart J, Sjögren RJO, Lundell LS, et al. Altered miR-29 expression in type 2 diabetes influences glucose and lipid metabolism in skeletal muscle. *Diabetes*. 2017;66:1807-1818.
50. Li J, Cen B, Chen S, He Y. MicroRNA-29b inhibits TGF-β1-induced fibrosis via regulation of the TGF-β1/Smad pathway in primary human endometrial stromal cells. *Mol Med Rep*. 2016;13:4229-4237.
51. Bae HJ, Noh JH, Kim JK, et al. MicroRNA-29c functions as a tumor suppressor by direct targeting oncogenic SIRT1 in hepatocellular carcinoma. *Oncogene*. 2014;33:2557-2567.
52. Adoro S, Cubillos-Ruiz JR, Chen X, et al. IL-21 induces antiviral microRNA-29 in CD4 T cells to limit HIV-1 infection. *Nat Commun*. 2015;6:7562. https://doi.org/10.1038/ncomms8562.
53. Elmén J, Lindow M, Schütz S, et al. LNA-mediated microRNA silencing in non-human primates. *Nature*. 2008;452:896-899.
54. Lanford RE, Hildebrandt-Eriksen ES, Petri A, et al. Therapeutic silencing of microRNA-122 in primates with chronic hepatitis C virus infection. *Science (80-)* 2010;327:198-201.
55. Alexander MS, Casar JC, Motohashi N, et al. MicroRNA-486-dependent modulation of DOCK3/PTEN/AKT signaling pathways improves muscular dystrophy-associated symptoms. *J Clin Invest*. 2014;124:2651-2667.
56. Baptista IL, Silva WJ, Artioli GG, et al. Leucine and HMB differentially modulate proteasome system in skeletal muscle under different sarcopenic conditions. *PLoS ONE*. 2013;8:e76752. https://doi.org/10.1371/journal.pone.0076752.
57. Bradford MM. A rapid and sensitive method for the quantitation of microgram quantities of protein utilizing the principle of protein-dye binding. *Anal Biochem*. 1976;72:248-254. https://doi.org/10.1016/0003-2697(76)90527-3.
58. Pereira MG, Baptista IL, Carlassara EOC, Moriscot AS, Aoki MS, Miyabara EH. Leucine supplementation improves skeletal muscle regeneration after cryolesion in rats. *PLoS ONE*. 2014;9:e85283.
59. Chan S, Head SI. Age- and gender-related changes in contractile properties of non-atrophied EDL muscle. *PLoS ONE* 2010;5(8):e12345. https://doi.org/10.1371/journal.pone.0012345.
60. Williams PE, Goldspink G. Longitudinal growth of striated muscle fibres. *J Cell Sci*. 1971;9:751-767.

SUPPORTING INFORMATION

Additional supporting information may be found online in the Supporting Information section at the end of the article.

How to cite this article: Silva WJ, Graça FA, Cruz A, et al. miR-29c improves skeletal muscle mass and function throughout myocyte proliferation and differentiation and by repressing atrophy-related genes. *Acta Physiol*. 2019;226:e13278. https://doi.org/10.1111/apha.13278